WWW.IJRPR.COM

International Journal of Research Publication and Reviews

Journal homepage: www.ijrpr.com ISSN 2582-7421

Study of Structural Characteristics of Erbium doped Yttrium Iron Garnet by Conventional Ceramic Method.

Muhammad Waqas[1], Zubair Khan[2], Usman Ali Qazi[3]

[1]Department of Physics, Government Postgraduate College Haripur, The University of Haripur.
[2] Department of Physics, Government Postgraduate College Haripur, The University of Haripur.
[3] Department of Physics, Government Postgraduate College Haripur, The University of Haripur.

ABSTRACT.

This article covered the traditional ceramic process for synthesizing Polycrystalline Erbium Doped Yttrium Iron Garnet nanoparticles ($Er_xY_{3-x}Fe_5O_{12}$)where x=0.6.The connection between Erbium concentration and sample characteristics can be readily illustrated by studying peers' results for x=0.1 and x=0.3. The stoichiometric combination is ($Er_xY_{3-x}Fe_5O_{12}$) where, x=0.6 blended by grinding and calcinated at 1100°C for one hour. For more purity sample is made into pellets and finally sintered at 1400°C for 2 hours. X-Ray Diffraction XRD and scanning electron microscopy SEM were used to evaluate the sample's detailed characteristics. The desired phase for the sample was achieved with the highest peak at (420) plane using XRD. Except for the deformation of one minor YFe_2O_3 peak caused by a strong bonding between iron and yttrium, all peaks are clearly defined and crisp. The structural properties of the (420) plane were examined. It is noticed that when Erbium concentration increases, the lattice constant and d-spacing decrease. It is also observed that the crystallite size does not vary greatly due to the almost similar ionic radii of Yttrium and Erbium. Because of the high sintering temperature, the grain size for all three samples is almost equal and quite big.

1. Introduction

The term ferrite comes from the Latin word "ferrum," which means "iron." Ferrites are magnetic materials that have both electrical and magnetic characteristics. The ferrites' major elements are iron oxide and metal oxides. For many ages, mankind has recognized the significance of ferrite material. The Chinese were able to utilize lodestones (Fe_3O_4) in compasses for navigation in the early 12th century [1]. Spinal ferrites, hexagonal ferrites, and garnets are the three basic types of ferrites. Spinal ferrites have the chemical formula $MOFe_2O_3$ or MFe_2O_4, where M denotes divalent cations (Mn, Fe, Ni, Zn, Mg, and Cd, for example). Oxygen atoms create a closed pack shape in the spinal lattice. The typical formula for hexagonal structure is $MFe_{12}O_{19}$, where M might be (Pb, Ba, or Sr). They were used as permanent magnetic materials [2]. The standard formula for magnetic rare earth garnets is $M_3Fe_5O_{12}$, where M might be Yttrium or any of the rare earth ions. The total magnetic moments of garnets can be altered through substitution. Magnetic memories (bubble memory) and microwave systems use substituted rare earth garnet. Spinal and garnet crystal formations are cubic, but hexaferrites crystal structures are hexagonal [3].

This paper discussed the microstructural aspects of ferrites. A ferromagnetic insulator known as yttrium iron garnet ($Y_3Fe_5O_{12}$), which Bertaut and Forrat discovered in 1956[4], was dubbed the "fruit fly of magnetism" by Kittel almost 50 years ago [5]. Yttrium iron garnet has a specific composition as well as a complex crystal structure with nearly cubic symmetry. YIG has a density of 5.17 g/cm^3 [6]. It has an extremely low magnetization damping of just 310-5 [7]. It has a large band gap of 2.85 eV and a high Curie temperature of roughly 560K. The lattice constant of the YIG unit cell is 12.376 ±0.004°A. O^h10-Ia3d is the most likely space group for yttrium iron garnet [8]. The YIG unit cell has a cubic structure and eight chemical formula units of $Y_3Fe_5O_{12}$ with a total of 160 ions (Figure 1.1). Each YIG formula unit has three dodecahedral (c site), two octahedral (a site), and three tetrahedral (d site) sites having 24 Y^{3+}, 40 Fe^{3+} , and 96 O^{2-} ions [9]. The Y^{3+} ions fill dodecahedral sites (c sites), which are surrounded by eight O^{2-} ions, forming an eight-cornered twelve-sided polyhedron. The 24 Fe^{3+} ions occupy tetrahedral sites (d sites) and are surrounded by four O^{2-} ions, resulting in tetrahedral symmetry. The 16 ions of Fe^{3+} occupy octahedral sites (a sites) and are surrounded by six O^{2-} ions, resulting in octahedral symmetry as shown in figure 1.1 [10].

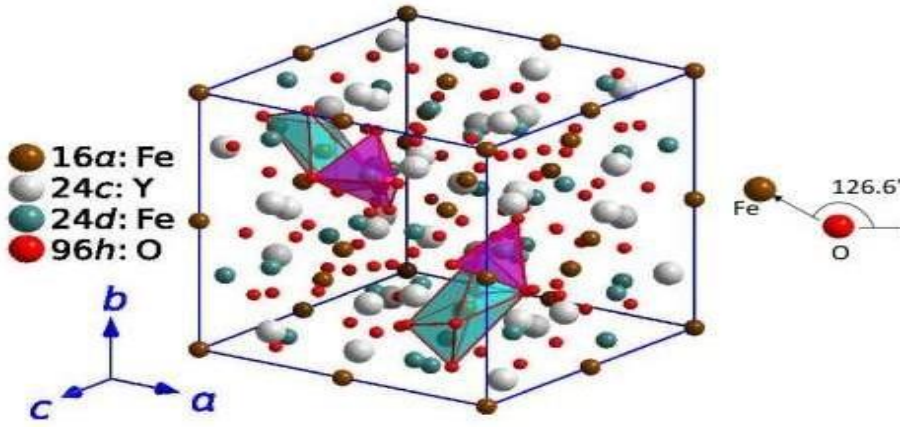

Figure 1.1 Crystal Structure of Yttrium iron garnet ($Y_3Fe_5O_{12}$) [11].

The microstructural aspect, Grain size affects the permeability. Studies reveal that less grain boundaries there are, the bigger the grains and the higher the permeability. This idea is often applicable to metallic magnetic materials. It has been said that grain size is not an important part of high permeability metallic materials such as Permalloy (an 80% Ni-Fe alloy) [12]. In recently published findings indicate that the lengths between pores account for variations in permeability. Even though the distances between pores were the same, samples with massive grains and porosity due to excessive grain development exhibited greater permeabilities than those with regularly developed grains [13]. Experiments also revealed that insufficient binder burn-off can result in a duplex structure. This research demonstrated the emergence of the duplex structure, as well as a degradation of magnetic characteristics, including a drop in permeability and an increase in losses [14].

Ferrites are regarded to be superior magnetic materials over pure metals due to their greater magnetism properties, high resistance, low cost, and simplicity of manufacture [15]. Sensors for alternating current and direct current magnetic fields, as well as alternating current and direct current electric currents, can be built. Nickel ferrite (Ni_{1-x} $Zn_xFe_2O_4$ with x = 1–0.5) lead zirconate-titanate ($PbZr_{0.52}Ti_{0.48}O_3$) sensors have demonstrated outstanding performance [16].

2. Methods and Materials

2.1 Chemical Used:

Erbium oxide Er_2O_3 powder with 99.99% purity (PanReac Application). Iron oxide Fe_2O_3 powder with 99.99% purity (Sigma Aldrich). Yttrium oxide Y_2O_3 powder with 99.99% purity (Sigma Aldrich) was used for the synthesis of Erbium substituted Yttrium Iron Garnet $Er_xY_{3-x}Fe_5O_{12}$ where x=0.6

There are several techniques to make Erbium substituted Yttrium Iron Garnet. However, the solid state reaction route is the most often used method for producing polycrystalline solids from a mixture of solid starting materials. At room temperature, solids do not react together on typical time scales. In order for the reaction to proceed at a significant pace, they must be heated to considerably higher temperatures, frequently ranging from 1000°C to 1500°C [17]. The typical chemical equation for obtaining Erbium substituted YIG is as follows:

$$\frac{3-x}{2}Y_2O_3 + \frac{x}{2}Er_2O_3 + \frac{5}{2}Fe_2O_3 \longrightarrow Er_xY_{3-x}Fe_5O_{12} \qquad \text{Eq (2.1)}$$

The value of x can be varied from zero to three (0-3). The chemical equation Eq (2.2) was used to get $Er_{0.6}Y_{2.4}Fe_5O_{12}$ substituting x = 0.6 in Equation (2.2) to get desired results.

$$\frac{(2.4)}{2}Y_2O_3 + \frac{0.6}{2}Er_2O_3 + \frac{5}{2}Fe_2O_3 \longrightarrow Er_{0.6}Y_{2.4}Fe_5O_{12} \qquad \text{Eq (2.2)}$$

We put x=0.6 in Eq (2.2). Only 10g of sample is required, so to get 10g sample of $Er_{0.6}Y_{2.4}Fe_5O_{12}$ stoichiometric calculation is done and the Reduction Factor is 78.

2.2 Working:

The preparation procedure for Erbium-substituted Yttrium Iron Garnet (Er: YIG) can be carried out using the following steps:

For $Er_{0.6}Y_{2.4}Fe_5O_{12}$

Initial material	**Molecular weight(g)**	**Weight for chemical reaction**	**Weight for initial compound of 10g**
Y2O3	225.809g	270.9708g	3.4739g
Er2O3	382.515g	114.7545g	1.4172g
Fe2O3	159.678g	399.2175g	5.1181g
Total		784.9428g	10.0632g

Table 2.1: Figure for 10g composition of $Er_{0.6}Y_{2.4}Fe_5O_{12}$

The stoichiometric measurement was performed on a 10g Er-YIG sample with an Erbium concentration of 0.6. The sample was then grinded for 2 hours to ensure homogeneous mixing of powder components. A homogenous mixture is required to achieve equal a mixture of Er ions in the final product. After mixing, the powder mixture is placed into a crucible and heated in a furnace under a controlled atmosphere. The heating profile involves ramping the temperature gradually from room temperature to 800°C at a rate of 5°C/min, holding at 800°C for 4 hours, then ramping up to 1100°C at a rate of 5°C/min. After sintering, the pellets are cooled to room temperature inside the furnace.

Different techniques are used for structural analysis however XRD is an essential technique for analyzing the crystal structure and to determine the substitution location of Erbium atoms in the YIG lattice of Erbium-substituted Yttrium Iron Garnet (Er: YIG). However, the XRD settings and parameters can have an important effect on the quality and accuracy of the findings [18]. Bragg's law illustrates the relation between the YIG crystal's X-ray wavelength, diffraction angle, and lattice spacing. Bragg's law may explain the lattice spacing and structure phases preferred crystal orientation as well as other structural factors such as grain size and crystallinity by measuring the diffraction angle and the X-ray wavelength [19].

SEM is a technique used to investigate the microstructure and surface morphology of the material. In the case of erbium doped YIG (yttrium iron garnet) the Er: YIG samples' SEM pictures revealed a variety of microstructural characteristics, including grain boundaries, pores, and cracks [20], the distribution of grain sizes was found to be rather consistent, with an average grain size of about 2µm. The grain boundaries appeared to be well-defined, showing that the material had a high degree of crystallinity. The existence of pores and cracks was also discovered, indicating that the sintering process may have resulted in certain material flaws. In addition to the microstructural characteristics, the SEM pictures revealed information on the material's composition [21, 22].

3. Results and Discussions

The phase of the sample is determined using XRD. The interaction of incident X-rays with the sample causes constructive interference, which satisfies Bragg's law. The wavelength of incoming X-rays is related to the diffraction angle and the distance between atomic planes in crystalline samples by Bragg's equation. Lattice parameter a of cubic YIG for all samples was calculated using the relation;

$$a = \sqrt{\left\{\frac{\lambda^2}{4\sin^2\theta}(h^2 + k^2 + l^2)\right\}} \qquad \text{Eq (3.1)}$$

Where λ (1.5405°A) is the wavelength, θ is the Bragg's angle in radian for given peaks, and [h k l] are Miller indices of respective peaks.

3.1 X-ray Analysis:

The XRD data of the sample is observed by an XRD machine called D8 Diffractometer. The XRD was collected by step scanning over the angular range of $20^0 \leq 2\theta \leq 80^0$. The data files are extracted by using Origin Pro Software (2016). The diffraction peaks for ($Er_{0.6}Y_{2.4}Fe_5O_{12}$) nanoparticles sintered at 1400°C are shown in Figure.3.1 and all the peaks list data and d-spacing which are calculated by using Bragg's law and results also shown in table 3.1. Maximum intensity was observed at $2\theta = 32.20$ at planes of (420). They are well define and sharp peaks are observed except a small peak of #$YFeO_3$ (Yttrium Iron Pervoskite) at $2\theta = 33.14$ in the given sample, it is due to strong bonding between iron and yttrium.

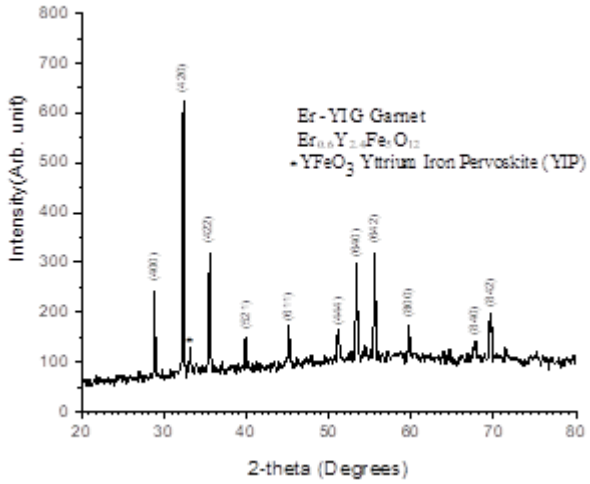

Figure 3.1 X-ray diffraction pattern of $Er_{0.6}Y_{2.4}Fe_5O_{12}$

Position (2Θ)	Height(Intensity)	FWHM(β) (Radians)	d-spacing (^{0}A)
28.92	141.6	0.00384	3.084852
32.39	329.6	0.003142	2.76185
35.58	206.3	0.003142	2.5212
53.43	224.2	0.004363	1.71348
55.61	188.7	0.004887	1.651361
69.60	152.8	0.003491	1.348191

Table 3.1: Peak list of $Er_{0.6}Y_{2.4}Fe_5O_{12}$ where x = 0.6

For the calculation of average crystallite size D we use the characteristics of (420) XRD peaks using the Scherrer formula.

$$D = \frac{C\lambda}{\beta cos\theta}$$

- **λ= 0.15405nm** is the wavelength incident x-ray.
- **β** is the relative value of full width half maximum (FWHM) of diffraction peak (420).
- θ Is the Bragg's angle at 2θ scale. Angles are taken in radian.

The lattice parameter, crystallite size, d-spacing, and molecular weight of $Er_{0.6}Y_{2.4}Fe_5O_{12}$ at (420) plane as shown in table 3.2

X	Position (2Θ)	Molecular Weight (g)	d-spacing (^{0}A)	Crystallite size (nm)	Lattice Constant (^{0}A)
0.6	32.39	784.9428	2.76185	45.95271	12.27554

3.2: Table Physical properties of $Er_{0.6}Y_{2.4}Fe_5O_{12}$ at (420) plane

3.2 SEM analysis

The grain size of the sample was done by using Scanning Electron Microscope (SEM). The SEM micrograph for $Er_{0.6}Y_{2.4}Fe_5O_{12}$ is express below, well defined and localized grains of uniform nature were observed in the micrograph. This magnified micrograph at 10μm clearly shows the grain of Erbium (0.6) YIG. The grain size was measured by using Image J software along with histogram to display the count rate, as results are shown in Table 3.3

Length (µm)	Mean	Minimum	Median	Maximum
	3.85462	0.894	3.608	8.147

Table 3.3: Variation of Grain size (µm) of $Er_{0.6}Y_{2.4}Fe_5O_{12}$

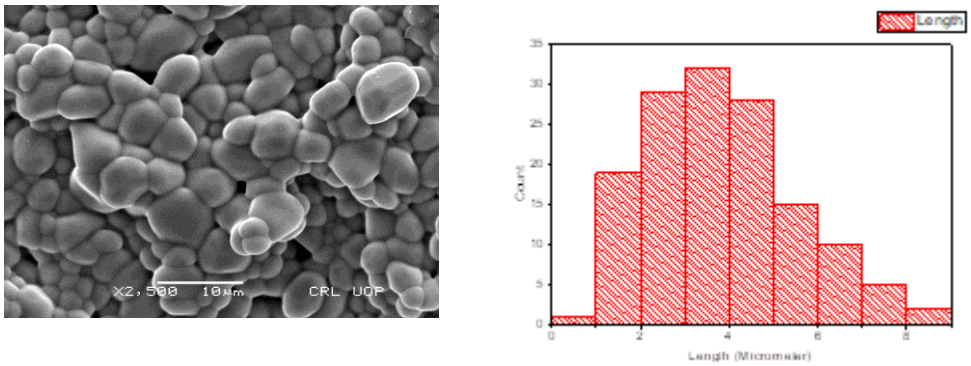

Figure 3.2 Micrograph and histogram of $Er_xY_{3-x}Fe_5O_{12}$

Comparison of Results of $Er_xY_{3-x}Fe_5O_{12}$ where x = 0.1, 0.3, 0.6. The results were compared of Erbium substituted Yttrium Iron Garnet ($Er_xY_{3-x}Fe_5O_{12}$) at concentration of x =0.6 with fellows which take the same sample but change its concentration such as take x = 0.1, 0.3.

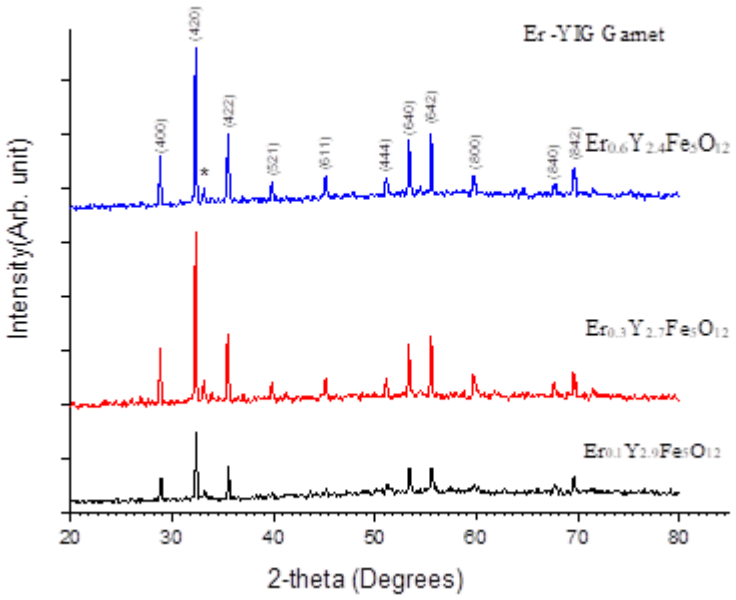

Figure 3.3 Comparison of X-ray diffraction pattern of $Er_xY_{3-x}Fe_5O_{12}$ where x = 0.1, 0.3 ,0.6

The d-spacing, lattice constants and crystallite sizes for (420) peaks are shown in Table 3.4;

X	**Position (2Θ)**	**Molecular Weight (g)**	**d-spacing (^{0}A)**	**Crystallite size (nm)**	**Lattice Constant (^{0}A)**
0.1	**32.33**	**745.7662**	**2.766838**	**45.94573**	**12.29798**
0.3	**32.34**	**761.4368**	**2.766005**	**48.65694**	**12.29423**
0.6	**32.39**	**784.9428**	**2.76185**	**45.95271**	**12.27554**

Table 3.4: Physical properties of $Er_xY_{3-x}Fe_5O_{12}$ at (420) plane

The lattice parameters from diffraction pattern of $Er_xY_{3-x}Fe_5O_{12}$ where x = 0.1, 0.3, 0.6 for (420) plane are calculated by using equation

$$a = \sqrt{\left\{\frac{\lambda^2}{4\sin^2\theta}(h^2 + k^2 + l^2)\right\}} \qquad \text{Eq (3.2)}$$

This decrease in lattice constant with increase in Erbium content at a single sintering temperature of 1400°C is due to replacement of smaller Erbium ion (crystal ionic radius of 1.03°A) by slightly larger Yttrium ion (crystal ionic radius 1.04°A) at dodecahedral sites of YIG unit cell.

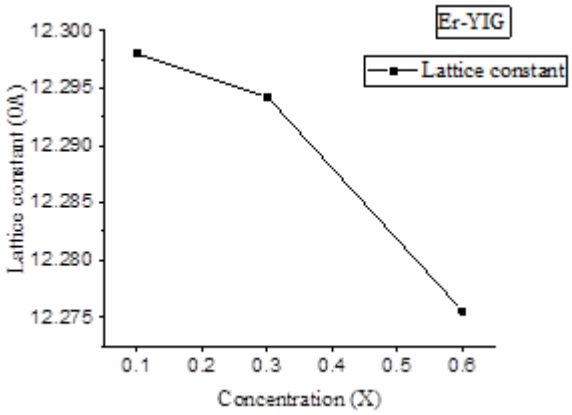

Figure 3.4 variation of lattice parameter of $Er_xY_{3-x}Fe_5O_{12}$ with Erbium (X).

The decrease in d-spacing is due to decrease in lattice constants as shown from table 3.4, same reduction in d-spacing is shown in Figure 3.5, further shift of XRD peaks to higher angles (2θ) with substitution of Erbium results the decrease in d-spacing as calculated from Bragg's law

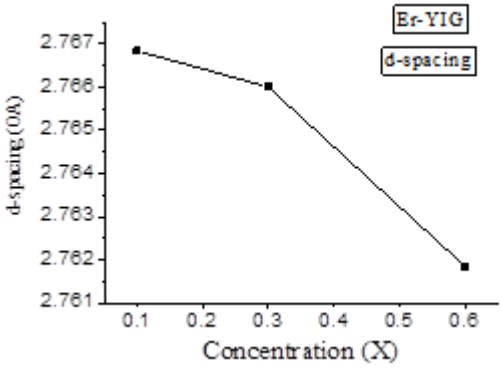

Figure 3.5 Variation of d-spacing of $Er_xY_{3-x}Fe_5O_{12}$ with Erbium (x)

It is observed that crystallite sizes are almost identical at same sintering temperature of 1400°C, it is probably due to almost identical effective ionic radii of Erbium ion (0.89°A) and Yttrium ion (0.90°A). To calculate the size of the crystallite for (420) peak Scherrer formula is used and values are in table 3.4. The variations are shown in figure 3.6.

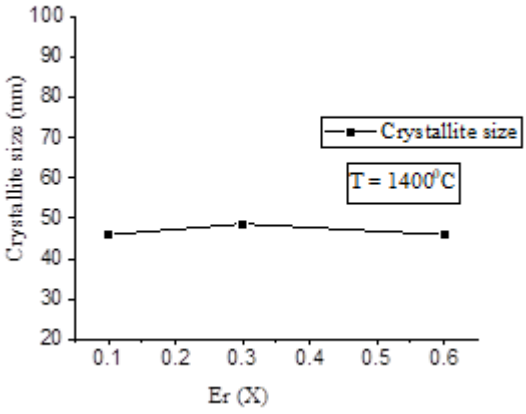

Figure 3.6 Variation of Crystallite size (nm) of $Er_xY_{3-x}Fe_5O_{12}$ with Erbium (x)

It is observed that average grain sizes for each sample slightly shift toward lower size as shown in Figure 3.7, it may be attributed to structural deformation i.e. due to decrease in Fe-O bond length with substation of Erbium at same sintering temperature of 1400°C. The average sizes of grains are large due to the very high sintering temperature of 1400°C.

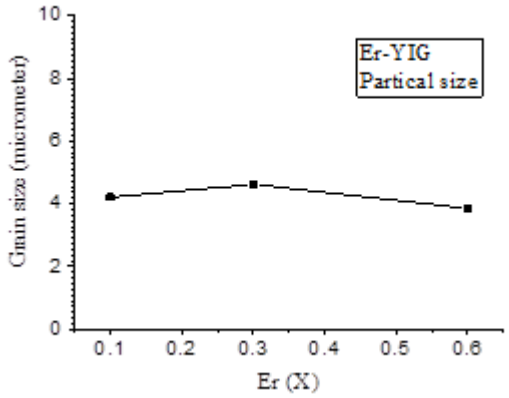

Figure 3.7: Variation of Grain size (μm) of $Er_xY_{3-x}Fe_5O_{12}$ with Erbium (x)

4. Summary and conclusions.

The article presents the preparation and structural characteristics of Erbium Doped Yttrium Iron Garnet nanoparticles ($Er_xY_{3-x}Fe_5O_{12}$)where x=0.6 .It was synthesized by Conventional Ceramic method using oxides (Y_2O_3, Er_2O_3, Fe_2O_3) powders as precursors. The XRD pattern confirms the formation of phases of cubic YIG. The highest peak was observed to be (420) plane. A small distort peak of $YFeO_3$ (Yttrium Iron Perovskites) is observed in all samples due to strong bonding between iron and yttrium. The XRD and SEM results showed that,

The variation in Erbium concentration in Er_xY_{3-x} Fe_5O_{12} brought a change in lattice constant. As Erbium concentration increases d-spacing decreases which in turn reduces lattice constant. Lattice constant decrease with increase in Er concentration at same sintering temperature of 1400°C is due to replacement of greater ionic radii (0.90°A) of Yttrium ion with smaller ionic radii (0.89°A) of Erbium ion. The lattice constant can be increased if Yttrium is substituted in a cubic unit cell the Fe-O bond length increases which in turn increases d-spacing. The increment in Erbium content moves the XRD peaks to the higher angles (2Θ). According to Bragg's law, angle varies inversely with d-spacing. XRD peaks shift to higher angle resulting in decrease in d-spacing.

Crystallite size shows non-linear variation for erbium content from 0.1 to 0.6. It ranges from 45.94nm - 48.65nm at the same sintering temperature of 1400°C. The small variation in crystallite size is due to almost equal ionic radii of Y and Er.The SEM result shows minute non-linear variation in grain sizes for Er content the observed grain size was in the range of (4.20951μm - 3.85462μm). The average sizes of grains are large but it cannot be observed due to nearly equal ionic radii of Yttrium 'Y' and substituted Erbium 'Er'.

References:

[1] J. Smit and H. P. J. Wijn Ferrites (Philips Technical Library, Eindhoven, 1959).

[2] Verma, R. C., & Singh, P. K. (2015). Ferrite materials: preparation, properties, and applications. CRC Press.

[3] Richa Srivastava, B.C. Yadav "Ferrite Materials: Introduction, Synthesis Technique, And Applications as Sensors". 4:141-154, 2012.

[4] F. Bertaut and F. Forrat, "The structure of the ferrimagnetic rare earth ferrites," Compt. rend. (1956), 242, 382-4., 1956.

[5] P. E. Wigen, R. D. McMichael, and C. Jayaprakash, "Route to chaos in the magnetic garnets," Journal of Magnetism and Magnetic Materials, vol. 84, no. 3, pp. 237–246, 1990.

[6] D. D. Stancil and A. Prabhakar, Spin Waves. Springer US, 2009.

[7] M. Sparks, Ferromagnetic-relaxation theory. McGraw-Hill advanced physics monograph series, McGraw-Hill, 1964.

[8] S. Geller and M. A. Gilleo, "Structure and ferromagnetism of yttrium and rare earth-iron garnets," Acta Crystallographica, vol.

[9] Goldman, A. (2006). Yttrium iron garnet (YIG) properties and applications. Journal of Applied Physics, 100(1), 011101.

[10] D. Badahur, Current Trends in Applications of Magnetic Ceramic Materials, Bull. Mater. Sci. 15 (1992) 431-439.

[11] M.Jungfleisch, "Wellenvektor Aufgelöste Brillouin-Lichtstreu Spektroskopie .

[12] Tebble, R.S. (1969) and Craik, D.J., Magnetic Materials, John Wiley and Sons, New York, 556

[13] Drofenik, M. (1985) Besenicar,S. and Limpel, M. Advances in Ceramics, 16^ 229

[14] Yoneda, N. (1980) Ito, S. and Katoh, I, Ceramic Bull, 59,549

[15] Pandey, R. S. (2017). Ferrites: Fundamentals and applications. Springer.

[16] Kausar Javaid Khan, Farhat Saleemi, Tahir Abbas, Farooq Bashir, Siara Riaz, Naseem Shahzad ``Microstructural and Magnetic Properties of Holmium Substituted Yttrium Iron Garnets ($Y_{3-x}H0_xFe_5O_{12}$)" Synthesized by Conventional Ceramic Method" Journals of Materials Today: Proceedings, Vol. 2, PP.5491-5496. (2015).

[17] "Solid State Chemistry and its Applications" Anthony R. West, Willey and Sons, 2005.

[18] Kumar, P., Kumar, P., & Kumar, S. (2019). Structural and magnetic properties of Er_{3+} substituted $Y_3Fe_5O_{12}$ (Er: YIG) nanoparticles prepared by solid-state reaction. Materials Today: Proceedings, 18, 1828-1834.

[19] Kumar, P., Kumar, P., & Kumar, S. (2019). Structural and magnetic properties of Er^{3+}substituted $Y_3Fe_5O_{12}$ (Er: YIG) nanoparticles prepared by solid-state reaction. Materials Today: Proceedings, 18, 1828-1834.

[20] Banerjee, A., Satpathy, S. K., & Agrawal, D. C. (2008). Microstructure and optical properties of erbium-doped yttrium iron garnet thin films deposited by sol–gel spin coating method. Journal of Applied Physics, 103(4), 044107.

[21] Ramesh, P., Krishnan, R. V., Sethupathi, K., & Santhosh, P. N. (2012). Structural and morphological studies of erbium doped yttrium iron garnet thin films using SEM and AFM. Journal of Materials Science: Materials in Electronics, 23(3), 528-533.

[22] Tobar, M. E., Ivanov, E., Cavin, J. D., & Camley, R. E. (1997). Scanning electron microscopy of erbium doped yttrium iron garnet thin films. Journal of Applied Physics, 81(8), 4341-4345.